

Symmetry-Breaking Charge Transfer in Metal–Organic Frameworks

Sreehari Surendran Rajasree,^a H. Christopher Fry,^b David J. Gosztola,^b Bapan Saha,^a Riya Krishnan,^a and Pravas Deria^{*a}

^aSchool of Chemical and Biomolecular Science, Southern Illinois University, 1245 Lincoln Drive, Carbondale, Illinois 62901, United States.

^bCenter for Nanoscale Materials, Argonne National Laboratory, 9700 S Cass Ave, Lemont, Illinois 60439, United States.

KEYWORDS.

ABSTRACT: High quantum-yield charge carrier generation from the initially prepared excitons defines a key step in the light-harvesting and conversion scheme. Photo-induced charge transfer in molecular electron donor-acceptor assemblies is driven by a sizable ΔG_0 , which compromises the potential of the generated carriers. Reminiscent of the special pair at the reaction center of the natural light-harvesting complex, symmetry-breaking charge transfer (SBCT) within a pair of identical struts will facilitate the efficient generation of long-lived charge carriers with maximized potentials without incorporating any foreign redox species. We report SBCT in pyrene-based zirconium MOF NU-1000 that leads to efficient radical ions in a polar solvent and bound CT state in a low polar solvent. The probe unveils the role of the low-lying non-Franck-Condon excitonic states as intermediates in the formation of the SBCT state from the initially prepared Franck-Condon S_1 states. Ultrafast and transient spectroscopy—probed over 200 fs–30 μ s timescale—evinces a $k_{SBCT} = (110 \text{ ps})^{-1}$ in polar media ($\epsilon_s = 37.5$) forming solvated radicals ions with recombination rate $k_{CR} = (\sim 45 \text{ ns})^{-1}$. A slower rate with $k_{SBCT} = (203 \text{ ps})^{-1}$ was recorded in low polar ($\epsilon_s = 7.0$) solvent manifesting a bound [TBAPy⁺⁺ TBAPy⁻] state with $k_{CR} \approx (17 \mu\text{s})^{-1}$. This discovery, along with other unique photophysical features relevant to light harvesting, should define a MOF-based platform for developing heterogeneous artificial photon energy conversion systems.

INTRODUCTION

Natural photosynthetic apparatus has provided us with an elegant blueprint of organized photosynthetic pigments for efficient solar energy conversion.^{1–3} Within the biological light-harvesting complex (LHC) the excited energy is anisotropically transported from the antennae to the special pair reaction center (RC) to generate charge carriers.^{2, 4} Maximizing the potential of these carriers, the RC splits the excitons through a unique strategy known as symmetry-breaking charge transfer (SBCT) within a pair of the identical but specifically oriented pair of chlorophylls ($Ch \cdots Ch + hv \rightarrow Ch^{\cdot+} + Ch^{\cdot-}$).⁵ This is in stark contrast to the common strategy of exploiting electronically asymmetric (donor-acceptor) pairs with a sizable driving force (ΔG_0), which compromises the potentials of the photo-generated charge carriers.⁶ While SBCT has been documented with a few molecular pigments in the homogeneous systems,^{7–14} they commonly lack various key features of LHC including panchromatic sensitization through a large portion of the visible spectrum,¹⁵ efficient and anisotropic delivery of the excitonic energy to the reaction center to produce long-lived redox equivalents.^{3, 16} Attempts to develop solid molecular compositions featuring most of these functionalities have commonly seen parasitic exciton recombination pathways.^{17–21}

Crystalline metal–organic frameworks (MOFs), built out of a wide range of photo- and redox-active pigment-based struts, offer a scalable solid-state foundation for developing artificial photosynthetic apparatus.^{22–26} Such foundations enable precise and periodic arrangement of the active/desired struts around geometrically well-defined pores, which not only suppress aggregation-mediated recombination (of excited state) but also provide means to modulate the excitonic properties and dynamics

relevant to their efficient delivery to ‘RC’ for photo-induced charge transfer (PCT) processes and catalytic utilities.^{27–29} Such developments have further been expanded by various post-synthesis approaches to install a wide range of complementary redox active entities.^{30–39}

Our works have established that MOF singlet excited states can be delocalized with molecular excitons spanning over multiple struts (that are built from aromatic cores like pyrene, porphyrin, phenyl-ethyne-phenyl, etc.).⁴⁰ Time-dependent density functional theory (TDDFT) based computations on small strut assemblies have enabled mapping of the transition density matrix (TDM) which evinced various excitonic states within the S_1 manifold including the initially prepared Franck-Condon (FC) excitonic state, denoted hereon as $S_1(\text{FC})$, are dispersed over multiple struts (evinced by the diagonal distribution of the excitonic mass. However, such interactions also manifest, within the S_1 manifold, low-energy non-Franck-Condon (NFC) excitonic states and they can be populated from the initial $S_1(\text{FC})$ due to a small energy gap and similar wave functions.^{29, 40, 41} While supramolecular assembly of electron donor-acceptor (D-A) motifs have been extensively exploited for PCT and their subsequent utilities^{6, 42–45} in the artificial light harvesting and conversion schemes,^{32, 40, 46} a systematic and transformative development underpinning the working principle to delineate the unique SBCT strategies in solid state system like MOF remained unaccomplished. While it is well perceived that the environment plays a critical role in modulating the energy of the SBCT state, spatial overlap of the frontier orbitals was established as a requirement for dimeric molecular systems.^{12, 47} Therefore, the dynamics of the SBCT state are tied with the molecular spacing and orientation—a feature that can be precisely defined and controlled by the pore geometry of MOFs which can also instigate a dielectric tuning. Given the spatially dispersed

MOF excitonic states, within the S_1 manifold, understanding the role of various NFC states during the $S_1(\text{FC}) \rightarrow \text{SBCT}$ process will provide unique insight and direction for further improving and developing MOFs-based energy conversion strategies.^{8, 48}

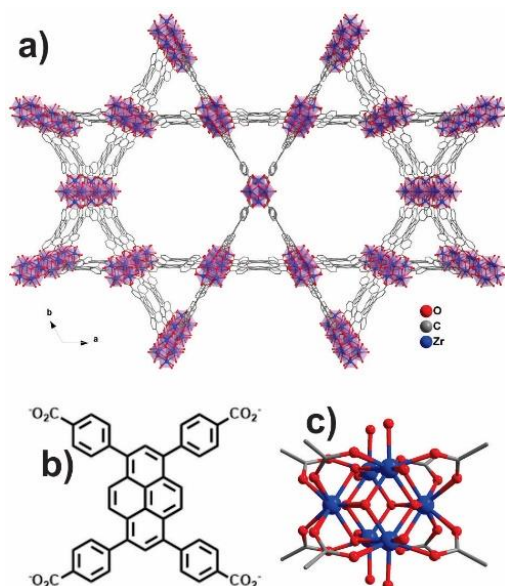


Figure 1. a) Chemical structure of NU-1000 and its constituent linker (b) TBAPy and (c) 8-connected Zr-oxo node. The structure highlights the hierarchical 1D pore system that anisotropically aligns the linkers along a triangular pore ($d=10 \text{ \AA}$) defining excitonic sites.⁴¹

RESULTS and DISCUSSIONS

PCT within an electronically asymmetric pair has been well established in pyrene [TBAPy: tetrabenzenecarboxypyrene]-based MOF NU-1000 with $k_{\text{PCT}} \sim (10\text{-}80 \text{ ps})^{-1}$. Owing to the large electronic driving force these systems compromise the potential energy of the charge carriers (leading to low redox strength or smaller V_{oc} in a photoelectrochemical setup) that recombine with $k_{\text{CR}} \sim (300 \text{ ps})^{-1}$.^{46, 49} However, pigment-pairs with comparable electronic potentials have been shown to undergo efficient PCT and slower recombination through exciplex-like intermediate.⁵⁰ Such systems are commonly achieved by post-synthetic installation of foreign redox components. Charge carrier generation through SBCT in MOFs featuring spatially dispersed singlet excitons with high and anisotropic mobility will define a significant step forward in artificial photosynthetic systems.

To achieve SBCT within the MOF assemblies of electronically isotropic struts (e.g., all pyrene-based MOFs), the pigment core must possess certain electronic features predicted from the Weller equation:^{51, 52}

$$\Delta G = e(E_{\text{ox}} - E_{\text{red}}) - E_{00} - C - S \quad (1)$$

$$[C \propto 1/\epsilon_s r_{LL} \text{ and } S \propto (1/r_+ - 1/r_-)]$$

where E_{ox} and E_{red} are the electrochemically determined oxidation and reduction potentials; $E_{0,0}$ is first excitation energy;⁵³ C and S are the Coulombic interactions between the two ions and their solvation correction terms. Coulombic interaction is inversely dependent on the solvent dielectrics. From these, it is expected that a small driving force can arise from the Coulombic term if the anionic radius (r_-) is larger than the cation (r_+).

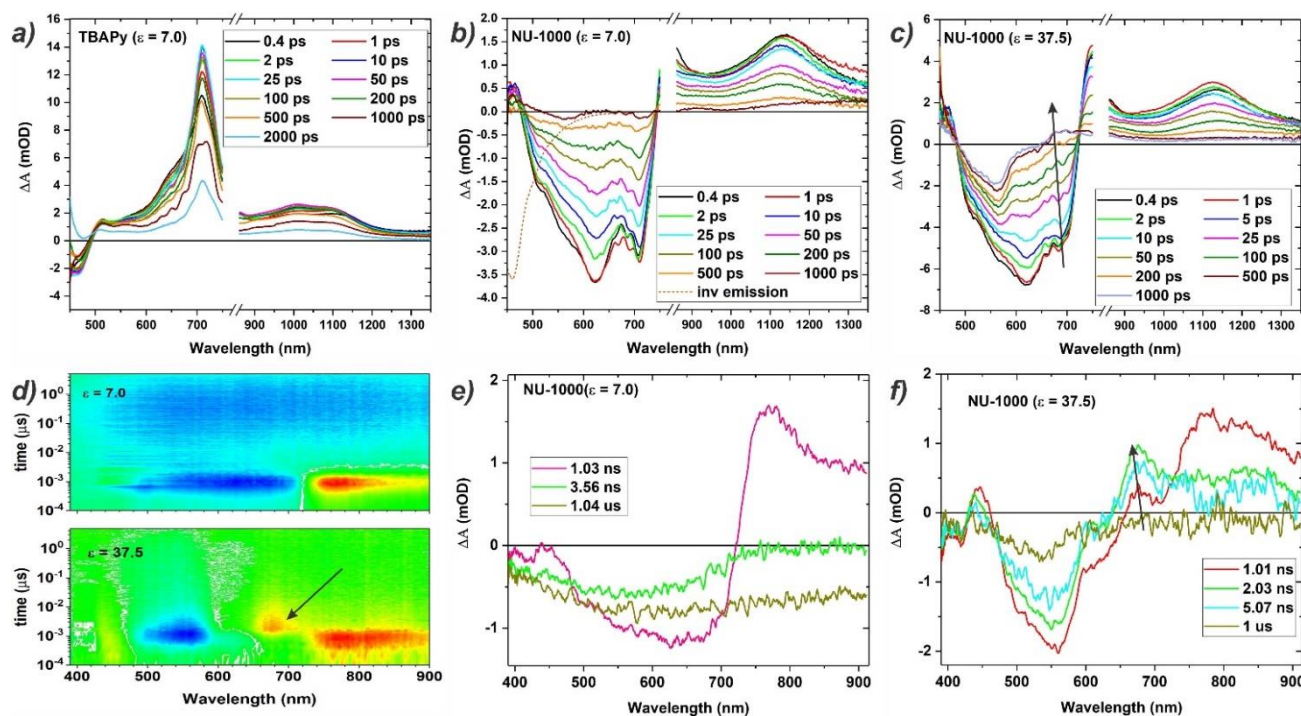


Figure 2. Dielectric dependent transient absorption spectra: a) fs-TA spectra of Et_4TBAPy in MeTHF solvent showing the $S_1 \rightarrow S_n$ transitions at 710 and broad 1000-1100 nm region (b) NU-1000 in a low polar solvent (dotted line is inverted emission) showing 500-725 nm SE from NFC states, (c) NU-1000 in polar solvent showing quick decay of the SE at $\sim 650\text{-}700 \text{ nm}$ region (arrow) due to appearance of positive TA signal for TBAPy^{++} and TBAPy^{--} radical ions (d) Color map for ns-TA of NU-1000 showing the evolution of SE from SBCT state in low polar and TA-signal (arrow) of radical ions formed in polar solvent. (e and f) are corresponding ns-TA spectra at various delay times showing the narrow bleaching band caused by the rise of radical ion signal (arrow).

In brief, an increase in solvent polarity will make the later term more negative to facilitate the CT process. From the Weller equation, a sizable driving force can be obtained for struts whose optical bandgap is slightly larger than their electrochemical bandgap. Screening various aromatic pigment-based MOFs, TBAPy- assembly of NU-1000 (Figure 1a) was picked for that the experimentally measured $E_{0,0} = 2.83$ eV; $E_{ox} - E_{red} = 2.09$ V; and $r_{LL} \sim 10.9$ Å. From these metrics ΔG of -0.88 and -0.9 eV as well as solvent reorganization energy, λ_s^{54} of 1.10 eV and 0.75 eV can be estimated in $\epsilon = 7.0$ (e.g., MeTHF) and $\epsilon = 37.5$ (e.g., MeCN, DMF) solvents.⁵⁵ Considering solvent independent internal reorganization energy ($\lambda_i = 0.39$ eV), a relative contribution of the exponential term in the Marcus rate equation^{56, 57} can be obtained using

$$k_e \propto H_{CT}^2 \exp \left[-\frac{(\lambda_i + \Delta G^0)^2}{4\pi\lambda_t k_B T} \right] \quad (2)$$

This indicated that the k_e in $\epsilon = 7.0$ solvent can be *ca* 1.25× larger than that in $\epsilon = 37.5$ media assuming a constant H_{CT} ($= \langle \psi_{SBCT} | \hat{H}_{CT} | \psi_{S_1(FC)} \rangle$, which is the electronic coupling matrix element for precursor and product states). Here, λ_t is the total reorganization energy ($= \lambda_i + \lambda_s$).

To probe SBCT in NU-1000, solvent-dielectric dependent (ϵ : ~7-38) transient spectroscopic experiments were carried out. Figure 2 displays the respective data. The femtosecond transient absorption (fs-TA) data collected for the unassembled TBAPy (ester form) strut in solution ($\epsilon = 7.0$; MeTHF) display an intense excited state absorption (ESA) at 710 nm and a broad NIR ESA in the 900-1200 nm region with a monotonous single species-based dynamics ($\tau = 2$ ns; Figure 2a). In contrast, the spectral signature of NU-1000 in $\epsilon = 7.0$ medium evinced that the initially prepared $S_1(FC)$ population (evinced by the red-shifted $S_1 \rightarrow S_n$ transitions appearing at ~750-850 nm and 1150 nm), which quickly (<0.4 ps) populates an ensemble of low-energy NFC states characterized by the broad (500 -750 nm) SE bands appearing significantly lower than the spontaneous emission band (at 470 nm, with shoulders at

500 and 550 nm; Figure 2b). The entire spectral envelope of SE from the NFC states recovers—followed further through the nanosecond transient absorption spectroscopy (ns-TA)—eventually to a species with a featureless broad spectral envelope of SE signal that spans beyond 920 nm. This long-lived state is insensitive to oxygen quenching (Figures S5, S6) and recombines over 15 μ s. Based on these, the long-lived featureless band is assigned to an SBCT state that can be envisioned as a bound [TBAPy⁺ TBAPy⁻] pair. Global fitting of the transient spectroscopic data (both fs-TA and ns-TA; See SI sec F) provides $\tau = 14$ ps, 203 ps, 1 ns, and 17 μ s time constants in MeTHF solvent. Based on the emissive lifetime (~1 ns) and quantum yield (~45%); a sizable $S_1(FC)$ population will continue displaying the $S_1 \rightarrow S_n$ signal causing a mixed state spectral signature in the EAS/SAS plots) these lifetimes can be attributed to $\tau[S_1(FC) \rightarrow NFC] = 14$ ps; $\tau[NFC \rightarrow SBCT] = 203$ ps, emissive decay $\tau[S_1 \rightarrow GS] = 1$ ns; and $\tau[SBCT \rightarrow GS] = 17$ μ s. The SBCT state did not manifest any spectral signature for radical ion species.

In contrast, the spectral evolution of TBAPy assemblies within NU-1000 in polar solvent ($\epsilon = 37.5$) was significantly different: The ensemble of NFC state efficiently populated to the SBCT state which partly manifests solvated radical ions as, at early stage, evinced by an unsymmetrical recovery of the broad SE band due to a quicker disappearance of low energy side with the emergence of an ESA signal at ~680 nm (Figure 2c) for the radical ions.^{46, 58} The radical ion signature can be seen in the ns-TA mapping data (Figure 2d), which caused a narrow leftover SE emission band (Figure 2f). Similar global fitting of the transient spectroscopic data collected in MeCN solvent provides [See SI sec F] time constants attributed to $\tau[S_1(FC) \rightarrow NFC] = 11$ ps; $\tau[NFC \rightarrow SBCT] = 110$ ps, emissive decay $\tau[S_1 \rightarrow GS] \approx 2$ ns (see Figure S4 for fluorescence lifetimes and Figures S7, S8 for the fit); and two time-constants for the recovery of the SBCT states: one from the radical ion pair $\tau[SBCT(\text{radical}) \rightarrow GS] \approx 45$ ns and from the bound pair with broad featureless SE, $\tau[SBCT \rightarrow GS] \approx 6.5$ μ s (Figure S10). Within the Marcus framework (eq 2), reorganization energy plays a dominant role for space-separated donor-acceptor pairs (from a

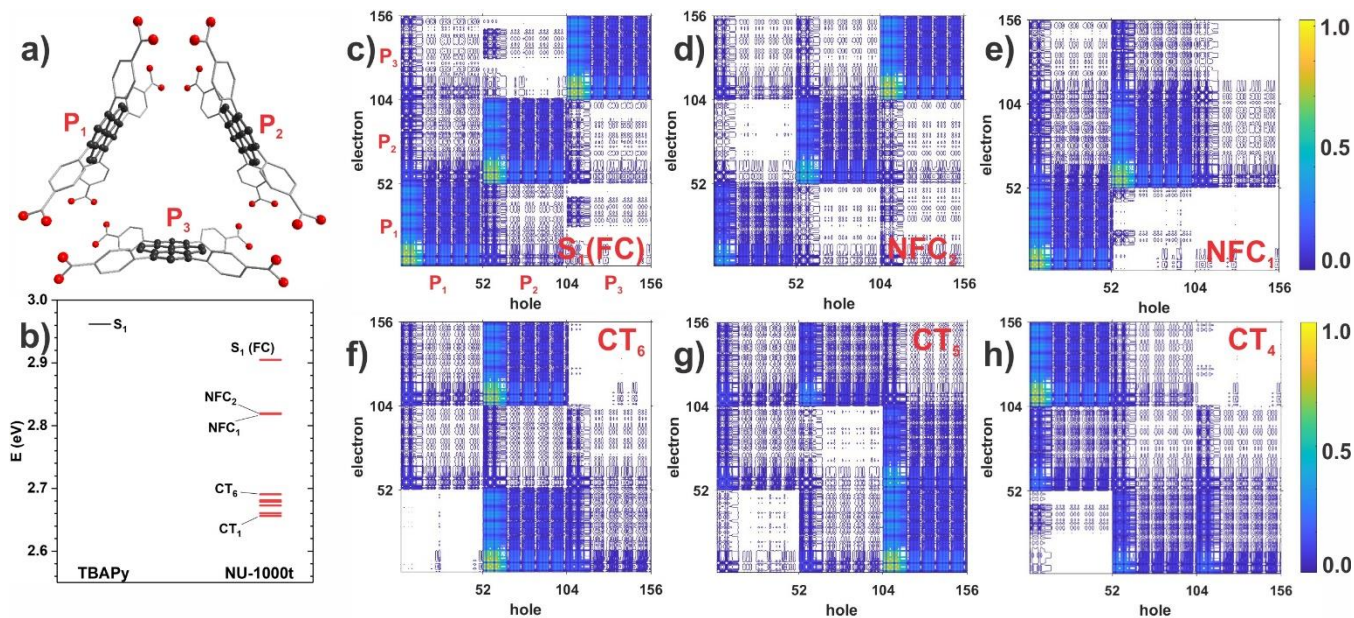


Figure 3. a) A trimeric TBAPy assembly of NU-1000 used for TDDFT computation proving the (b) energy for the $S_1(FC)$, NFC, and CT states at the GS-optimized geometry; the S_1 energy for an unassembled TBAPy strut is given for comparison. Contour plots of TDMs for various excited states: (c) $S_1(FC)$ (marked P_i are the TBAPy strut shown in panel (a), each with 52 atoms as numbered in the axes), (d-e) NFC states and (e-f) CT_6 , CT_5 , and CT_4 states. The colors represent the densities normalized to 1.

neutral D^{*}-A/D-A^{*} pair in the S₁(FC) state to a charge pair D⁺-A⁻ in the SBCT state) predicting an efficient process in low dielectric media. However, transient spectroscopic data indicates polar solvent not only facilitates the SBCT formation but can also stabilize the radical ion state. Since the S₁(FC) state in NU-1000 is delocalized over many TBAPy struts with excitonic sites defined by the three TBAPy struts around each triangular pore, the process can be considered as a radiation-less transition of the initially prepared S₁(FC) population to the SBCT state of a given superchromophore,⁴¹ and will scale with $\exp\left[-(\Delta E_{S_1(FC)-SBCT} - \lambda)^2/\lambda\right]$. This transition will be further facilitated by the involvement of a low energy NFC intermediate state with small reorganization and $\Delta E_{NFC-SBCT}$ energy gap (i.e., S₁(FC) → NFC → SBCT). For that an efficient S₁(FC) → NFC transition was observed with $\tau \sim 11$ -15 ps owing to a small $\Delta E_{S_1(FC)-NFC}$.

To shed some light on the excited state species, a small triangular model consisting of three TBAPy struts—defining one excitonic site—was used for TDDFT (See SI sec G for details) computation.⁴¹ The TDDFT computed energies on the ground state (GS) optimized structure (i.e., vertical excitation) of these excitonic states are plotted in Figure 3b. Based on the oscillator strengths and corresponding excitonic mass distribution in the respective TDM plots, the ninth state was assigned as the S₁(FC), right below which (8th and 7th) are the two NFC states named NFC₁ and NFC₂ and followed by six SBCT states, CT₆-CT₁ (Figure 3b).⁵⁹ The excitonic mass distribution in the respective TDM plots (Figure 3d-e) suggests that the NFC₁ and NFC₂ states can be described as $|^1(P_1 P_2 P_3)^*$, $|^1(P_1 P_2)^* P_3$, and so on; where P₁, P₂, and P₃ are the adjacent TBAPy pigments in a triangular model (Figure 3a). Notably, the NFC₂ ($|^1(P_1 P_2)^* P_3$) state⁶⁰ describes an excimer-like complex that can be a good precursor for the SBCT state.⁶¹ Among the six lower energy SBCT states, only CT₄ (Figure 3h) denotes an ionic state described by $|P_1^+ P_2 P_3^- \rangle$ with asymmetrically distributed (non-diagonal) excitonic mass and the rest of the CT_n states can be described as partial charge-distributed states, like $|P_1^+ P_2^{\delta-} P_3^- \rangle$, $|P_1^{\delta+} P_2^{\delta+} P_3^- \rangle$, and so on (Figures 3 and S13).

The NFC → SBCT transitions can be understood from the energies of the excited state (ES) relaxed geometry (i.e., TDDFT/opt),⁸ where among the six CT_n states the highest energy CT₆ can be considered as the initial transition point from the lowest energy NFC₁ state. For the S₁(FC) → NFC → SBCT transition, the energy variation for the respective states was probed: the $\Delta E_{S_1(FC)-NFC} = 0.058$ eV at GS-optimized structure, which increases (0.11 eV) at the ES-optimized geometry at which a nominal $\Delta E_{NFC-CT_6} = 6 \times 10^{-3}$ eV was found (Figure S14, S15).⁴⁸ It is therefore clear that despite a sizable energy gap between the initial S₁(FC) and final SBCT states, the NFC state, as an intermediate, can tunnel the population: it has a small energy gap with the initially prepared S₁(FC) state at the GS-optimized geometry (i.e., upon the vertical excitation) and a small gap with the SBCT state upon relaxation. TDDFT based ES-optimization implementing polarizable continuum model for different dielectric media (THF and MeCN) suggests that the energies of the (see Figure S15) CT₄ state is significantly stable in a polar solvent and destabilized in a nonpolar solvent which also feature a larger $\Delta E_{NFC-CT_6} = 11 \times 10^{-3}$ eV (compared to that evinced for $\epsilon = 37.5$). This explains the observation of a faster SBCT formation rate (100 ps⁻¹) leading to radical ion signature in polar solvent ($\epsilon = 37.5$) where low dielectric media can only manifest SE from the bound partially polarized states. Based on these computational and experimental data the processes were summarized in Figure 4 and Figure S16.

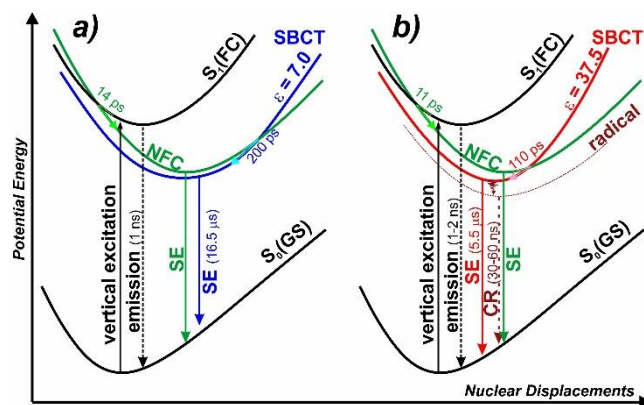


Figure 4. Potential energy surfaces describing the excited state processes involved in SBCT in NU-1000 in (a) low ($\epsilon = 7$) and (b) high ($\epsilon = 37.5$) polar solvents. See Figure S15 for the TDDFT computed energies at the GS and ES-optimized structures.

CONCLUSIONS

Interchromophoric interaction within the MOF-assembled organic pigment/struts gives rise to several excitonic states within the S₁ manifold including the initially prepared Franck-Condon excitonic states, S₁(FC), and lower-energy non-Franck-Condon (NFC) excitonic states -which can be populated from the initial S₁(FC). The extent of the excitonic mass distribution and respective nuclear coordinates varies for these states: for example, while the S₁(FC) states are spatially dispersed, some of the low-energy NFC states can be anisotropic defining excimer-like and CT states. Pigment-based struts with $E_{0,0} > E_{redox}$ and with anionic radius (r_-) is larger than the cation (r_+) could produce SBCT states, whose energy and potential surface can be modulated by the dielectric environment defined by the infiltrated solvent, whereas the inter-pigment interaction and, therefore, the dynamics of the SBCT states can be dictated by the pore geometry. Within this context, pyrene-assembled NU-1000 showed efficient SBCT formation. While predicted observations from classic electron transfer theory suggested that a low dielectric media can be beneficial for SBCT formation, transient spectroscopic results evince that polar solvent not only facilitates the SBCT formation but can also stabilize the radical ion state. Given that the initially prepared S₁(FC) state in NU-1000 is delocalized over many TBAPy struts with excitonic sites defined by the three TBAPy struts around each triangular pore, the S₁(FC) → SBCT transition can be described as a radiation-less transition between two states where involvement of NFC state plays a critical role tunneling the population owing to the small energy gap and reorganization energy at the GS-structure (for S₁(FC) → NFC) and excited state relaxed structure (for NFC → SBCT). Time-dependent DFT computation suggests the formation of various SBCT states defined by the variable extent of asymmetric charge distribution, among which the radical ion pair state is more stable in polar solvent enabling spectroscopic identification. In polar media, the efficient formation ($k_{SBCT} = (110 \text{ ps})^{-1}$) of the persisting radical ion state ($k_{CR} = (45 \text{ ns})^{-1}$) represents a remarkable feature for developing artificial photosynthetic solids within such MOFs forming long-lived usable charge carriers. The discovery, therefore, highlights a rich vein of unique photophysics that has been eluding in solid compositions: SBCT in MOF can be modular by the optoelectronic property of the pigment itself and by the pore geometry of the frameworks that precisely defines and controls the inter-pigment distance and orientation. Such structural

features not only enable exceptionally mobile spatially dispersed singlet excitons but can dictate how they will be split –i.e., the dynamics of the SBCT and the extent of charge-transfer (radical ions vs bound pairs) even within MOFs constructed from a given pigment –corollary that is simply difficult to achieve in solution dissolved macromolecular systems.

ASSOCIATED CONTENT

Supporting Information. Experimental details, computational, and additional spectroscopic data. This material is available free of charge via the Internet at <http://pubs.acs.org>.

AUTHOR INFORMATION

Corresponding Author

* Pravas Deria

pderia@siu.edu.

ACKNOWLEDGMENT

P.D. gratefully acknowledges funding from the National Science Foundation (NSF CAREER CHE-1944903). Use of the Center for Nanoscale Materials, an Office of Science user facility, was supported by the U.S. Department of Energy, Office of Science, Office of Basic Energy Sciences, under Contract No. DE-AC02-06CH11357. SEM-EDS data were collected at the SIUC IMAGE center (supported by NSF grant #CHE0959568).

REFERENCES

- (1) Scholes, G. D.; Fleming, G. R.; Olaya-Castro, A.; Grondelle, R. v. Lessons from Nature about Solar Light Harvesting. *Nature Chemistry* **2011**, *3*, 763-774.
- (2) Damjanović, A.; Ritz, T.; Schulten, K. Energy transfer between carotenoids and bacteriochlorophylls in light-harvesting complex II of purple bacteria. *Physical Review E* **1999**, *59*, 3293-3311.
- (3) Barber, J.; Andersson, B. Revealing the Blueprint of Photosynthesis. *Nature* **1994**, *370*, 31-34.
- (4) Brinkert, K. *Energy Conversion in Natural and Artificial Photosynthesis*; Springer, 2018.
- (5) Deisenhofer, J.; Norris, J. R. *The Photosynthetic Reaction Center*; Academic Press, Inc., 1993.
- (6) Wasielewski, M. R. Photoinduced Electron Transfer in Supramolecular Systems for Artificial Photosynthesis. *Chem. Rev.* **1992**, *92*, 435.
- (7) Sebastian, E.; Hariharan, M. Symmetry-Breaking Charge Separation in Molecular Constructs for Efficient Light Energy Conversion. *ACS Energy Letters* **2022**, *7*, 696-711.
- (8) Piet, J. J.; Schuddeboom, W.; Wegewijs, B. R.; Grozema, F. C.; Warman, J. M. Symmetry Breaking in the Relaxed S1 Excited State of Bianthryl Derivatives in Weakly Polar Solvents. *J. Am. Chem. Soc.* **2001**, *123*, 5337-5347.
- (9) Fritz, R.; Rettig, W.; Nishiyama, K.; Okada, T.; Müller, U.; Müllen, K. Excitonic and Charge Transfer States in Oligomeric 9,10-Anthrylene Chains. *J. Phys. Chem. A* **1997**, *101*, 2796-2802.
- (10) Giaimo, J. M.; Lockard, J. V.; Sinks, L. E.; Scott, A. M.; Wilson, T. M.; Wasielewski, M. R. Excited Singlet States of Covalently Bound, Cofacial Dimers and Trimers of Perylene-3,4:9,10-bis(dicarboximide)s. *J. Phys. Chem. A* **2008**, *112*, 2322-2330.
- (11) Markovic, V.; Villamaina, D.; Barabanov, I.; Lawson Daku, L. M.; Vauthey, E. Photoinduced Symmetry-Breaking Charge Separation: The Direction of the Charge Transfer. *Angew. Chem. Int. Ed.* **2011**, *50*, 7596-7598.
- (12) Estergreen, L.; Mencke, A. R.; Cotton, D. E.; Korovina, N. V.; Michl, J.; Roberts, S. T.; Thompson, M. E.; Bradforth, S. E. Controlling Symmetry Breaking Charge Transfer in BODIPY Pairs. *Acc. Chem. Res.* **2022**, *55*, 1561-1572.
- (13) Whited, M. T.; Patel, N. M.; Roberts, S. T.; Allen, K.; Djurovich, P. I.; Bradforth, S. E.; Thompson, M. E. Symmetry-Breaking Intramolecular Charge Transfer in the Excited State of Meso-Linked BODIPY Dyads. *Chem. Commun.* **2012**, *48*, 284.
- (14) Sebastian, E.; Hariharan, M. Null Exciton-Coupled Chromophoric Dimer Exhibits Symmetry-Breaking Charge Separation. *J. Am. Chem. Soc.* **2021**, *143*, 13769.
- (15) Trinh, C.; Kirlikovali, K.; Das, S.; Ener, M. E.; Gray, H. B.; Djurovich, P.; Bradforth, S. E.; Thompson, M. E. Symmetry-Breaking Charge Transfer of Visible Light Absorbing Systems: Zinc Dipyrrins. *J. Phys. Chem. C* **2014**, *118*, 21834-21845.
- (16) Wasielewski, M. R. Photoinduced electron transfer in supramolecular systems for artificial photosynthesis. *Chem. Rev.* **1992**, *92*, 435-461.
- (17) Wasielewski, M. R. Self-Assembly Strategies for Integrating Light Harvesting and Charge Separation in Artificial Photosynthetic Systems. *Acc. Chem. Res.* **2009**, *42*, 1910-1921.
- (18) Prathapan, S.; Johnson, T. E.; Lindsey, J. S. Building-block synthesis of porphyrin light-harvesting arrays. *J. Am. Chem. Soc.* **1993**, *115*, 7519-7520.
- (19) Hasobe, T.; Kashiwagi, Y.; Absalom, M. A.; Sly, J.; Hosomizu, K.; Crossley, M. J.; Imahori, H.; Kamat, P. V.; Fukuzumi, S. Supramolecular Photovoltaic Cells Using Porphyrin Dendrimers and Fullerene. *Adv. Mater.* **2004**, *16*, 975-979.
- (20) Sengupta, S.; Würthner, F. Chlorophyll J-Aggregates: From Bioinspired Dye Stacks to Nanotubes, Liquid Crystals, and Biosupramolecular Electronics. *Acc. Chem. Res.* **2013**, *46*, 2498-2512.
- (21) Kim, D.; Osuka, A. Directly Linked Porphyrin Arrays with Tunable Excitonic Interactions. *Acc. Chem. Res.* **2004**, *37*, 735-745.
- (22) Feng, D.; Gu, Z.-Y.; Li, J.-R.; Jiang, H.-L.; Wei, Z.; Zhou, H.-C. Zirconium-Metalloporphyrin PCN-222: Mesoporous Metal-Organic Frameworks with Ultrahigh Stability as Biomimetic Catalysts. *Angew. Chem. Int. Ed.* **2012**, *51*, 10307-10310.
- (23) Mondloch, J. E.; Bury, W.; Fairen-Jimenez, D.; Kwon, S.; DeMarco, E. J.; Weston, M. H.; Sarjeant, A. A.; Nguyen, S. T.; Stair, P. C.; Snurr, R. Q.; Farha, O. K.; Hupp, J. T. Vapor-Phase Metalation by Atomic Layer Deposition in a Metal-Organic Framework. *J. Am. Chem. Soc.* **2013**, *135*, 10294-10297.
- (24) Jiang, H.-L.; Feng, D.; Wang, K.; Gu, Z.-Y.; Wei, Z.; Chen, Y.-P.; Zhou, H.-C. An Exceptionally Stable, Porphyrinic Zr Metal-Organic Framework Exhibiting pH-Dependent Fluorescence. *J. Am. Chem. Soc.* **2013**, *135*, 13934-13938.
- (25) Lan, G.; Li, Z.; Veroneau, S. S.; Zhu, Y.-Y.; Xu, Z.; Wang, C.; Lin, W. Photosensitizing Metal-Organic Layers for Efficient Sunlight-Driven Carbon Dioxide Reduction. *J. Am. Chem. Soc.* **2018**, *140*, 12369-12373.
- (26) Rajasree, S. S.; Li, X.; Deria, P. Physical properties of porphyrin-based crystalline metal-organic frameworks. *Commun. Chem.* **2021**, *4*, 47.
- (27) Li, X.; Surendran Rajasree, S.; Yu, J.; Deria, P. The Role of Photoinduced Charge Transfer for Photocatalysis, Photoelectrocatalysis and Luminescence Sensing in Metal-Organic Frameworks. *Dalton Transac.* **2020**, *49*, 12892-12917.
- (28) Deria, P.; Yu, J.; Smith, T.; Balaraman, R. P. Ground-State versus Excited-State Interchromophoric Interaction: Topology Dependent Excimer Contribution in Metal-Organic Framework Photophysics. *J. Am. Chem. Soc.* **2017**, *139*, 5973-5983.
- (29) Yu, J.; Anderson, R.; Li, X.; Xu, W.; Goswami, S.; Surendran Rajasree, S.; Mairdan, K.; Gómez-Gualdrón, D. A.; Deria, P. Improving Energy Transfer within Metal-Organic Frameworks by Aligning Linker Transition Dipole along Framework Axis. *J. Am. Chem. Soc.* **2020**, *142*, 11192-11202.

- (30) Karagiari, O.; Bury, W.; Mondloch, J. E.; Hupp, J. T.; Farha, O. K. Solvent-Assisted Linker Exchange: An Alternative to the *De Novo* Synthesis of Unattainable Metal–Organic Frameworks. *Angew. Chem. Int. Ed.* **2014**, *53*, 4530-4540.
- (31) Takaishi, S.; DeMarco, E. J.; Pellin, M. J.; Farha, O. K.; Hupp, J. T. Solvent-Assisted Linker Exchange (SALE) and Post-Assembly Metallation in Porphyrinic Metal–Organic Framework Materials. *Chem. Sci.* **2013**, *4*, 1509-1513.
- (32) Goswami, S.; Yu, J.; Deria, P.; Hupp, J. T. Light Harvesting “Antenna” Behavior in NU-1000. *ACS Energy Lett.* **2021**, *6*, 848-853.
- (33) Van Wyk, A.; Smith, T.; Park, J.; Deria, P. Charge-Transfer within Zr-Based Metal–Organic Framework: The Role of Polar Node. *J. Am. Chem. Soc.* **2018**, *140*, 2756-2760.
- (34) Williams, D. E.; Dolgoplova, E. A.; Godfrey, D. C.; Ermolaeva, E. D.; Pellechia, P. J.; Greytak, A. B.; Smith, M. D.; Avdoshenko, S. M.; Popov, A. A.; Shustova, N. B. Fulleritic Well-Defined Scaffolds: Donor–Fullerene Alignment Through Metal Coordination and Its Effect on Photophysics. *Angew. Chem. Int. Ed.* **2016**, *55*, 9070-9074.
- (35) Song, Y.; Li, Z.; Zhu, Y.; Feng, X.; Chen, J. S.; Kaufmann, M.; Wang, C.; Lin, W. Titanium Hydroxide Secondary Building Units in Metal–Organic Frameworks Catalyze Hydrogen Evolution under Visible Light. *J. Am. Chem. Soc.* **2019**, *141*, 12219-12223.
- (36) Lin, S.; Cairnie, D. R.; Davis, D.; Chakraborty, A.; Cai, M.; Morris, A. J. Photoelectrochemical alcohol oxidation by mixed-linker metal–organic frameworks. *Faraday Discuss.* **2021**, *225*, 371-383.
- (37) Liu, X.; Kozłowska, M.; Okkali, T.; Wagner, D.; Higashino, T.; Brenner-Weiß, G.; Marschner, S. M.; Fu, Z. Z., Q.; Imahori, H.; Bräse, S.; Wenzel, W.; Wöll, C.; Heinke, L. Photoconductivity in Metal–Organic Framework (MOF) Thin Films. *Angew. Chem. Int. Ed.* **2019**, *58*, 9590-9595.
- (38) Dolgoplova, E. A.; Rice, A. M.; Smith, M. D.; Shustova, N. B. Photophysics, Dynamics, and Energy Transfer in Rigid Mimics of GFP-based Systems. *Inorg. Chem.* **2016**, *55*, 7257-7264.
- (39) Choi, S.; Jung, W.-J.; Park, K.; Kim, S.-Y.; Baeg, J.-O.; Kim, C. H.; Son, H.-J.; Pac, C.; Kang, S. O. Rapid Exciton Migration and Amplified Funneling Effects of Multi-Porphyrin Arrays in a Re(I)/Porphyrinic MOF Hybrid for Photocatalytic CO₂ Reduction. *ACS Appl. Mater. Interfaces* **2021**, *13*, 2710-2722.
- (40) Yu, J.; Park, J.; Van Wyk, A.; Rumbles, G.; Deria, P. Excited State Electronic Properties in Zr-based MOFs as a Function of Topological Network. *J. Am. Chem. Soc.* **2018**, *140*, 10488-10496.
- (41) Rajasree, S. S.; Yu, J.; Pratik, S. M.; Li, X.; Wang, R.; Kumbhar, A. S.; Goswami, S.; Cramer, C. J.; Deria, P. Superradiance and Directional Exciton Migration in Metal–Organic Frameworks. *J. Am. Chem. Soc.* **2022**, *144*, 1396-1406.
- (42) Lee, C. Y.; Farha, O. K.; Hong, B. J.; Sarjeant, A. A.; Nguyen, S. T.; Hupp, J. T. Light-Harvesting Metal–Organic Frameworks (MOFs): Efficient Strut-to-Strut Energy Transfer in Bodipy and Porphyrin-Based MOFs. *J. Am. Chem. Soc.* **2011**, *133*, 15858-15861.
- (43) Dolgoplova, E. A.; Williams, D. E.; Greytak, A. B.; Rice, A. M.; Smith, M. D.; Krause, J. A.; Shustova, N. B. A Bio-inspired Approach for Chromophore Communication: Ligand-to-Ligand and Host-to-Guest Energy Transfer in Hybrid Crystalline Scaffolds. *Angew. Chem., Int. Ed.* **2015**, *54*, 13639-13643.
- (44) Fang, Z.-B.; Liu, T.-T.; Liu, J.; Jin, S.; Wu, X.-P.; Gong, X.-Q.; Wang, K.; Yin, Q.; Liu, T.-F.; Cao, R.; Zhou, H.-C. Boosting Interfacial Charge-Transfer Kinetics for Efficient Overall CO₂ Photoreduction via Rational Design of Coordination Spheres on Metal–Organic Frameworks. *J. Am. Chem. Soc.* **2020**, *142*, 12515-12523.
- (45) Xia, Z.; He, C.; Wang, X.; Duan, C. Modifying electron transfer between photoredox and organocatalytic units via framework interpenetration for β -carbonyl functionalization. *Nat. Commun.* **2017**, *8*, 1-11.
- (46) Van Wyk, A.; Smith, T.; Park, J.; Deria, P. Charge-Transfer within Zr-Based Metal–Organic Frameworks: The Role of Polar Node. *J. Am. Chem. Soc.* **2018**, *140*, 2756-2760.
- (47) Lee, C.; Choi, C. H.; Joo, T. A Solvent–Solute Cooperative Mechanism for Symmetry-Breaking Charge Transfer. *Phys. Chem. Chem. Phys.* **2020**, *22*, 1115.
- (48) Roy, P.; Bressan, G.; Gretton, J.; Cammidge, A. N.; Meech, S. R. Ultrafast Excimer Formation and Solvent Controlled Symmetry Breaking Charge Separation in the Excitonically Coupled Subphthalocyanine Dimer. *Angew. Chem. Int. Ed.* **2021**, *60*, 10568-10572.
- (49) Li, X.; Yu, J.; Gosztola, D. J.; Fry, H. C.; Deria, P. Wavelength-Dependent Energy and Charge Transfer in MOF: A Step towards Artificial Porous Light-Harvesting System. *J. Am. Chem. Soc.* **2019**, *141*, 16849-16857.
- (50) Li, X.; Yu, J.; Lu, Z.; Duan, J.; Fry, H. C.; Gosztola, D. J.; Mairan, K.; Surendran Rajasree, S.; Deria, P. Photoinduced Charge Transfer with a Small Driving Force Facilitated by Exciplex-like Complex Formation in Metal–Organic Frameworks. *J. Am. Chem. Soc.* **2021**, *143*, 15286-15297.
- (51) Rehm, D.; Weller, A. Kinetics of Fluorescence Quenching by Electron and H-Atom Transfer. *Isr. J. Chem.* **1970**, *8*, 259-271.
- (52) Weller, A. Photoinduced Electron Transfer in Solutions: Exciplex and Radical Ion Pair Formation Free Enthalpies and their Solvent Dependence. *Z. Phys. Chem.* **1982**, *133*, 93-98.
- (53) E_{0,0} values determined from the crossing point of their normalized lowest energy absorption and fluorescence spectra.
- (54) The solvent reorganization energy (λ_s) for the bulk solvent was calculated by the Marcus relation:⁵⁵
- $$\lambda_s = \frac{e^2}{4\pi\epsilon_0} \left(\frac{1}{2r_D} + \frac{1}{2r_A} - \frac{1}{r_{DA}} \right) \left(\frac{1}{n^2} - \frac{1}{\epsilon_s} \right)$$
- Where, ϵ_0 is the permittivity of free space, ϵ_s the static dielectric constant of the solvent, n is the refractive index, and e is the magnitude of the charge of an electron; r_+ and r_- are the effective radius of the cation (3.02 Å) and the anion (7.1 Å), respectively.
- (55) Marcus, R. A. On the Theory of Electron-Transfer Reactions. VI. Unified Treatment for Homogeneous and Electrode Reactions. *J. Chem. Phys.* **1965**, *43*, 679-701.
- (56) Coropceanu, V.; Cornil, J.; da Silva Filho, D. A.; Olivier, Y.; Silbey, R.; Brédas, J.-L. Charge Transport in Organic Semiconductors. *Chem. Rev.* **2007**, *107*, 926-952.
- (57) Marcus, R. A. On The Theory of Electrochemical and Chemical Electron Transfer Processes. *Can. J. Chem.* **1959**, *37*, 155.
- (58) Kung, C.-W.; Wang, T. C.; Mondloch, J. E.; Fairen-Jimenez, D.; Gardner, D. M.; Bury, W.; Klingsporn, J. M.; Barnes, J. C.; Van Duyne, R.; Stoddart, J. F.; Wasielewski, M. R.; Farha, O. K.; Hupp, J. T. Metal–Organic Framework Thin Films Composed of Free-Standing Acicular Nanorods Exhibiting Reversible Electrochromism. *Chem. Mater.* **2013**, *25*, 5012-5017.
- (59) a larger model, two triangular unit with six struts can be used with the expense of computation time resulting proportionally 36th state as the S₁(FC) which delocalized over all six TBAPy units forming two excitonic sites.
- (60) and other possible ones like $|^1(P_1^* P_2 P_3)\rangle$ in larger model
- (61) Miller, C. E.; Wasielewski, M. R.; Schatz, G. C. Modeling Singlet Fission in Rylene and Diketopyrrolopyrrole Derivatives: The Role of the Charge Transfer State in Superexchange and Excimer Formation. *J. Phys. Chem. C* **2017**, *121*, 10345-10350.

TOC graphic:

